Electrical Resistance Tomography Imaging of Spatial Moisture Distribution in Pavement Sections

OK-KEE KIM, WILLIAM A. NOKES, H. MICHAEL BUETTNER, WILLIAM D. DAILY, AND ABELARDO L. RAMIREZ

The Division of New Technology, Materials, and Research (NTM&R) of the California Department of Transportation sought a method to measure the spatial distribution and movement of moisture in a pavement section. Measurement of electrical resistivity was investigated because of the inverse relationship between resistivity and moisture content. NTM&R collaborated with Lawrence Livermore National Laboratory in applying electrical resistance tomography (ERT) to measure and subsequently image spatial resistivity. The results from two field experiments succeeded in showing images that correlate very well with layers in pavement sections. Images from sequential ERT measurements reveal water movement within the pavement and into the subgrade. Results suggest that ERT technology may be an important research tool in understanding moisture distribution and movement.

The Division of New Technology, Materials and Research (NTM&R) of the California Department of Transportation (Caltrans), sought a method to measure the spatial distribution and movement of moisture in a pavement section. Measurement of electrical resistivity, using electrical resistance tomography (ERT) was investigated because of the inverse relationship between resistivity and moisture content: high resistivity is interpreted as low moisture content and low resistivity is interpreted as high moisture content. NTM&R collaborated with Lawrence Livermore National Laboratory (LLNL) in evaluating ERT for measurement and subsequently for imaging. This paper presents a brief description of ERT technology and the results of two field experiments.

CONCEPT AND THEORY OF ERT

ERT is a method for determining the electrical resistivity distribution in a volume based on discrete measurements of current and voltage on the boundary. Resistivity data can be taken in a variety of configurations, including borehole to borehole or borehole to surface. Detailed technical concepts and theory used for ERT can be found elsewhere (*1*,*2*).

To obtain an image of the region between two boreholes, a number of electrodes are placed in each hole in electrical contact with the surrounding material. An aspect ratio of 2:1 for borehole depth to borehole spacing is common. A pair of adjacent electrodes is driven by a known current, and the resulting voltage difference is measured between other pairs of electrodes. The known current then is applied to another pair of electrodes, and the voltage is again measured between other pairs. This procedure is repeated until current has been applied to all pairs of electrodes (in both holes). The ratio of a voltage at one pair of terminals to the current causing it is a transfer resistance. For n electrodes there are $n(n-3)/2$ independent transfer resistances.

The next step is to calculate the distribution of resistivity between the boreholes given the measured transfer resistances and to construct an image. However, the calculation for the distribution of resistivity is highly nonlinear because the currents flow along the paths of least resistance and are dependent on the resistivity distribution. Finite element method (FEM) algorithms and least-squares methods are used to invert the transfer resistances.

Image construction can be on the same FEM mesh used to calculate the measurements or on a different array. An absolute image shows a resistivity structure, whereas a comparison image shows changes in resistivity with time. Comparison images can be used to study dynamic processes in pavement structure, such as percolation, by comparing data taken at different times. This paper presents both absolute images and comparison images.

Forward Solution

The forward solution to Poisson's equation uses FEM to compute the electrical potential response of a two-dimensional earth caused by a three-dimensional source. To avoid the difficulty of numerically solving a three-dimensional problem, Poisson's equation is formulated in the wave number domain via Fourier transformation in the strike direction. According to Hohmann (*3*), the governing equation is

$$\frac{\partial}{\partial x}\left(\sigma\frac{\partial V}{\partial x}\right) + \frac{\partial}{\partial z}\left(\sigma\frac{\partial V}{\partial z}\right) - \lambda^2\sigma V = -\mathrm{I}\delta(x)\,\delta(z) \qquad (1)$$

where

V = potential in Fourier transform domain,
σ = conductivity,
λ = the Fourier transform variable,
I = source current, and
$\delta(x)$ = delta function.

O-K. Kim, Division of New Technology, Materials and Research, California Department of Transportation, 5900 Folsom Blvd., Sacramento, Calif. 95819. W. A. Nokes, Division of State and Local Project Development, California Department of Transportation, 650 Howe Ave., Suite 400, Sacramento, Calif, 95325. H. M. Buettner, W. D. Daily, and A. L. Ramirez, Lawrence Livermore National Laboratory, P.O. Box 808, Livermore, Calif. 94551.

FIGURE 1 Location of experiment site.

The two-dimensional FEM algorithm is based on the theory described by Huebner and Thorton (*4*) and the implementation follows that described by Wannamaker et al. (*5*) for modeling two-dimensional magnetotelluric data. Using FEM, potentials are calculated for a discrete number of transform variables at the nodes of a mesh of quadrilateral elements. The potentials are then inverse transformed back into the Cartesian domain using the method described by LaBrecque (*6*).

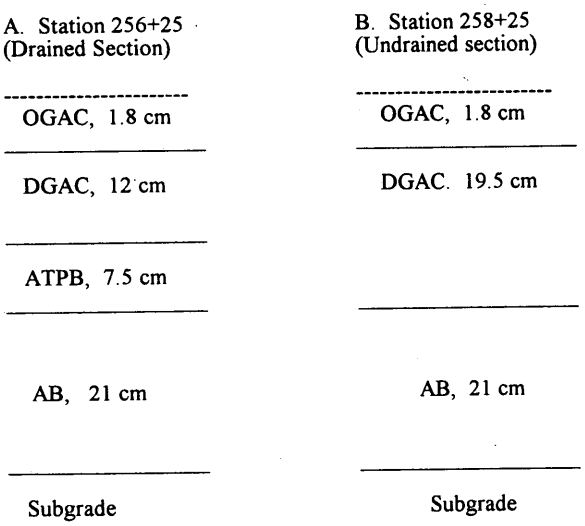

FIGURE 2 Pavement structural section of Experiment 1 site.

TABLE 1 Summary of Subgrade Soil Properties

Water content by weight, %	15.33
Dry bulk density of soil, gr/cc	1.72
Degree of saturation, %	70.9
Specific gravity of soil particle	2.73

Numerical Inversion

The inversion method uses the modified Marquardt algorithm (*7*) to jointly solve the nonlinear equation

$$\mathbf{WD} = \mathbf{W}*\mathbf{F(P)} \tag{2}$$

and the equation

$$\mathbf{P}^T\mathbf{RP} = 0 \tag{3}$$

where

D = vector of known data values,
W = weighting matrix,
P = vector of unknown parameters,
F(P) = the forward solution, and
R = the roughness matrix that is a numerical approximation to the Laplacian operator (*8*). To solve these equations jointly, the algorithm minimizes

$$\chi^2 + cL\,(\mathbf{P}) = 0 \tag{4}$$

where c is a constant and χ is the chi-squared statistic that is given by

$$[\mathbf{D}*\mathbf{F(P)}]^T\mathbf{W}^T\mathbf{W}[\mathbf{D}*\mathbf{F(P)}] = \chi^2 \tag{5}$$

Ideally the inverse algorithm would find the maximum value of c for which χ^2 is equal to some value known a priori. The constant (c) was determined by trial and error by calculating an inverse model with an a priori value of c and then adjusting (if necessary) to achieve the correct value of χ^2.

TABLE 2 Resistivity Test Results of Subgrade Soil (03-SUT-99, PM 4.9, Northbound, Sta. 256 + 25)

Water Content, % by Weight	Resistance (ohms)	Resistivity (ohm-cm)	
15.6	340	2322	
19.6	216	1475	
23.6	131	895	
27.6	110	751	
31.6	105	717	Minimum Resistivity
35.6	108	738	
39.6	110	751	
43.5	117	799	
55.5	120	820	

Resistivity = resistance*6.83

TABLE 3 Resistivity of Field Backfill Material

Station	Hole I.D.*	Resistance (ohms)	Resistivity (ohm-cm)
256+25 (Drained)	1	100,000	190,500
	2	160	304
258+25 (Undrained)	A	800	1,525
	B	80	152
	C	80	152

Hole I.D.* : corresponds to Figure 3.

TABLE 4 Mixing Formulation for Backfill Material

Mixing Components	Composition, % by Weight
Gravel (B-39)	47.2
Sand (B-11)	31.7
Coke breeze (DW-2)	10.2
Polyester resin	10.7
MEK (Methyl Ethyl Ketone)	0.2

FIELD EXPERIMENT

Experiment 1

Test Sites and Instrument Installation

Caltrans and LLNL researchers first installed ERT arrays on northbound Highway 99 near the Sacramento Metro Airport (shown as 03-SUT-99 in Figure 1) in December 1991. Test sites are located at stations 256 + 25 (built with a drainage layer) and 258 + 25 (without a drainage layer) on the outer (Number 2) lane. The elevation of the highway surface nearly equals that of the adjacent rice fields, which are usually filled with irrigation water from April to September and which typically are assumed to increase subgrade moisture during the dry summer.

Pavement cross sections in Figure 2 show similar designs. Station 256 + 25 has open-graded asphalt concrete (OGAC, 1.8 cm), dense-graded asphalt concrete (DGAC, 12 cm), asphalt-treated permeable base (ATPB, 7.6 cm), and aggregate base (AB, 21 cm) over subgrade soil. In contrast, station 258 + 25 has no ATPB (in Lane 2) and the DGAC is 19.5 cm thick. ATPB was inadvertently placed in Lane 1 at station 258 + 25 but was sealed with a slurry seal before placing the DGAC.

The subgrade soil at the test sites was sampled during construction for subsequent laboratory testing, which is summarized in Table 1. Soil from station 256 + 25 was used to measure resis-

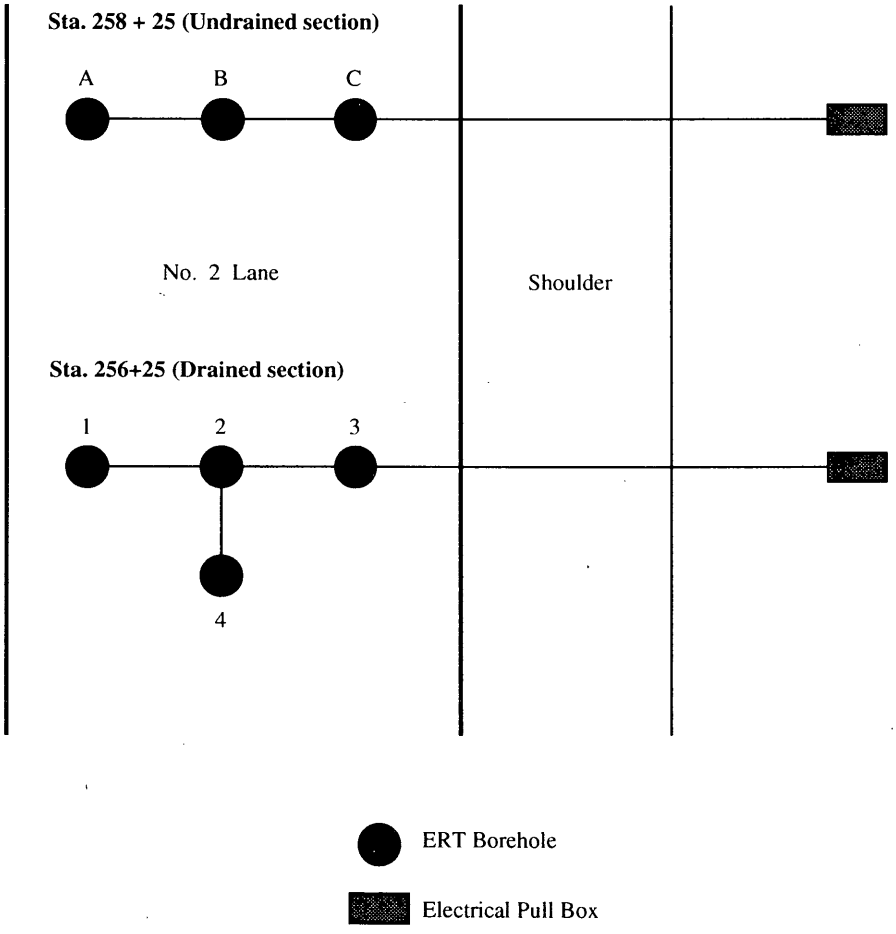

FIGURE 3 ERT layout at Experiment 1 site (note drawn to scale).

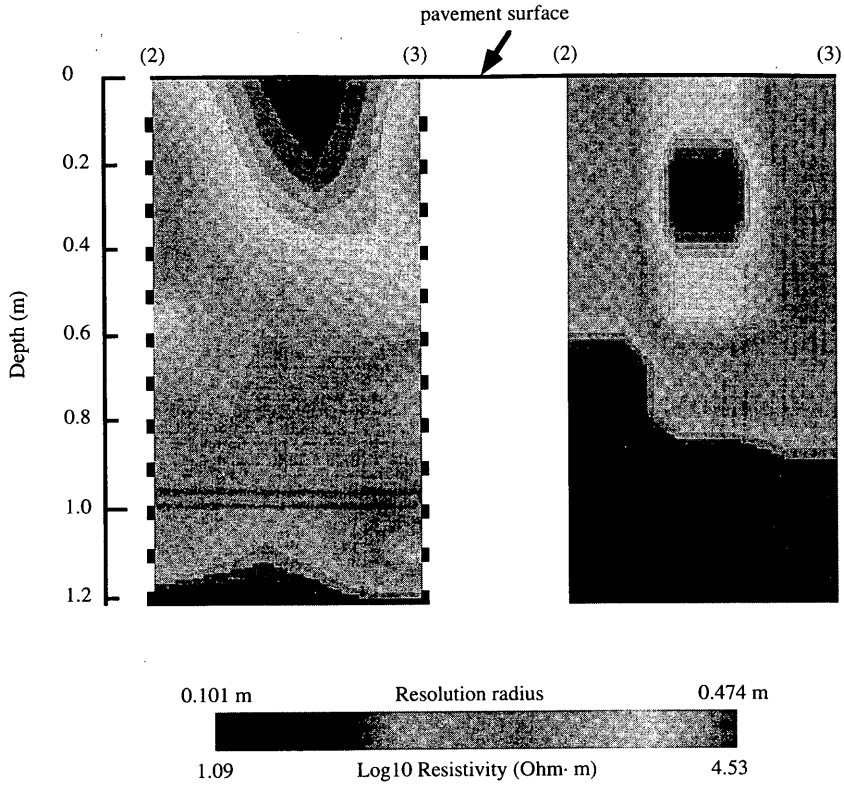

FIGURE 4 Absolute ERT image and resolution radius of Plane 2–3 for Experiment 1.

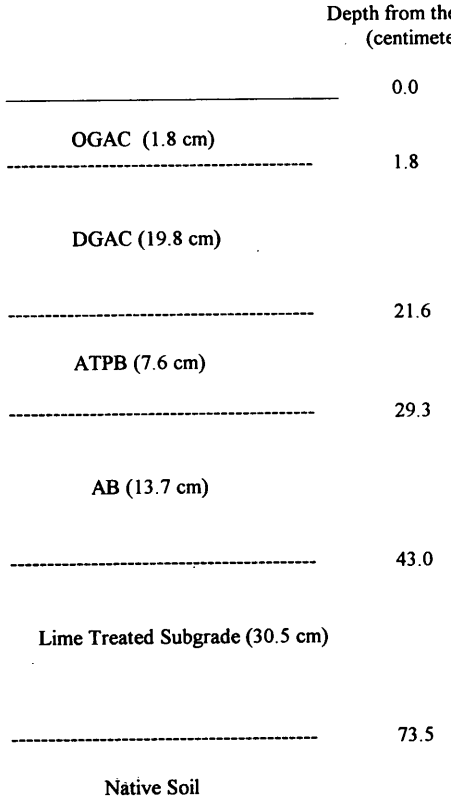

FIGURE 5 Pavement structural section of Experiment 2 site.

tivity on the basis of California Test Method 643 (*9*). Results shown in Table 2 show that resistivity ranges from 717 to 2322 ohm-cm depending on water content.

Conductive backfill material for ERT electrodes was prepared in the NTM&R laboratory and then mixed at the site using a small mechanical mixer. A nominal resistivity of 2000 ohm-cm was tar-

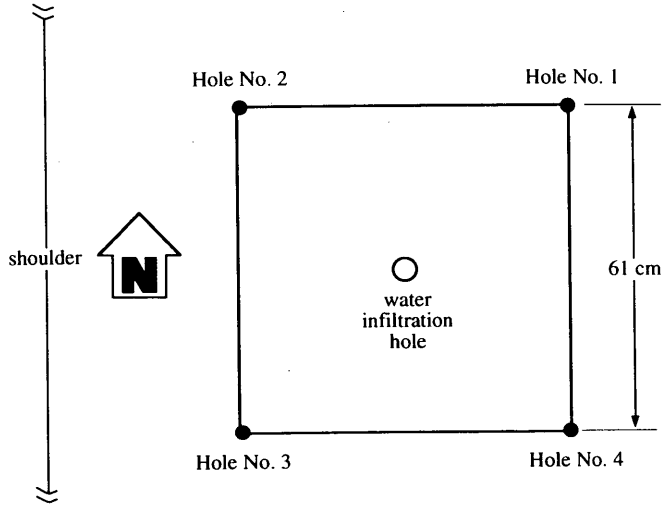

FIGURE 6 Layout of ERT boreholes for Experiment 2. Boreholes 1 and 2 were backfilled with the excavated native soil. LTS, AB, and cold AC patching material. Boreholes 3 and 4 were backfilled with cement-mortar and cold AC patching material.

geted for the backfill material surrounding the ERT arrays in each borehole. The backfill material was placed in the 3.8 cm ± annular space. Five-block specimens (7.5 × 7.5 × 30 cm) were made and brought back to the NTM&R laboratory to check the resistivity. The formulation of backfill material and its resistivity are presented in Tables 3 and 4.

The layout of ERT boreholes is shown in Figure 3. Spacing the holes 60 cm apart and 125 cm deep (each ERT array was 121.9 cm long) met the 2:1 aspect ratio requirement. Each hole diameter was 10 cm. Surface electrodes originally were to be placed in the AC surface layer, but stiff AC from the cold weather prevented installation.

Results and Discussion

The first two of three efforts to collect resistivity measurements yielded poor-quality data. LLNL researchers tried both sites, but data obtained from these two trips were insufficient for reconstructing images. The principal difficulties were (a) excessively high cross-hole resistance levels and (b) a dynamic range in the data too large for the measurement system to handle. The dynamic range refers to both the limits on injected current (1 amp maximum) and measured voltage (4 V maximum). Much of the data fell outside these limits.

On the third trip, in April 1992, the LLNL researchers tried to correct the difficulties mentioned above by (a) using higher drive voltages at the current injection electrodes and (b) splitting the measurement schedules into two parts to accommodate the large dynamic range of voltage measurements. It was necessary to break the measurement schedule into several parts, thus increasing the time required to collect data from both sites. A complete data set was collected for the plane between Boreholes 2 and 3, referred to as the "2–3" plane (see Figure 3), which resulted in an absolute image of resistivity shown in Figure 4. In the reconstruction, the dark end of the gray scale corresponds to low electrical resistivity (wet) and the light end to high resistivity (dry). The small solid rectangles on both vertical edges in the 2–3 plane indicate the location of electrodes spaced every 10 cm.

A distinct transition from high to low resistivity is shown in Figure 4 at a depth of about 40.6 cm below the pavement surface. This transition corresponds approximately to the boundary between the AB layer and the subgrade at 42.3 cm, as illustrated in Figure 3. The resistivity distribution in Figure 4 shows that, as expected, the upper layers are drier than the subgrade. It is difficult to interpret results further about the resistivity distribution in the plane 2–3 because the spatial resolution is no better than about 10 cm in the bottom of the plane and ranges from 30.5 to 50.8 cm in the upper part of Figure 4. Sampling for image reconstruction generally is better with smaller-resolution radius.

The poor resolution (or higher-resolution radius) is a consequence of the low-quality field data caused by backfill material having highly variable resistivity. Laboratory measurements shown in Table 3 show wide variations and nonlinearity in resistivity. Resistivity tests (called four-point measurements) on backfill material conducted at LLNL confirmed that the relationship between current and voltage was not linear. Undesirable properties were grossly evident when the LLNL researchers found that they could easily generate spark discharges and smoke at the current injection electrodes.

Experiment 2

Test Site and Installation

A second set of ERT electrodes was installed in September 1992 on the truck scale ramp just north of Riego Road on southbound Highway 99 (03-SUT-99). The site is located about 4 km south of the Experiment 1 sections and is built with OGAC (1.8 cm), DGAC (19.8 cm), ATPB (7.6 cm), AB (13.7 cm) and lime-treated subgrade (LTS, 30.5 cm) over native soil as illustrated in Figure 5.

Figure 6 shows a plan view of four boreholes 10.2 cm in diameter where electrode arrays were inserted. Four image planes were defined by four linear arrays of electrodes placed into holes at corners of a 61-cm square. The electrode arrays extended to 121.9 cm below the pavement surface. There are 12 electrodes in each hole and 5 surface electrodes on each edge of the square. Surface electrodes were placed into holes 1.3 cm in diameter drilled into the bottom of sawcuts (approximately 5.1 cm wide and 5.1 cm deep) on the pavement surface. These holes extended about 5.1 cm into the DGAC layer.

Electrodes in boreholes and at the surface were spaced every 10.2 cm. One hole 10.2 cm in diameter was drilled at the center of the square (see Figure 6) down to the bottom of the ATPB layer for a water infiltration experiment, which was conducted to better understand vertical and horizontal water flow.

Two kinds of backfill material were tried: cement mortar and excavated pavement materials. Cement mortar with a 1 to 3 ratio (by weight) was used with a water-cement ratio of 0.5. Boreholes 1 and 2 (see Figure 6) were backfilled with the excavated native soil, LTS, and AB materials, which were removed from the holes during drilling. Space in the ATPB, DGAC, and OGAC was filled with cold AC patching material. Boreholes 3 and 4 were filled with cement mortar up to the top of the aggregate base, and cold AC patching material filled the remaining space to the surface. A steel rod was used to compact the backfill materials to eliminate air pockets around the electrodes and to ensure good contact between the backfill materials and electrodes. Commercial concrete patching and cold AC patching materials were used to fill the sawcut trench.

Results and Discussion

Effect of Backfill Materials Measurements collected in March 1993 provided better-quality data than did the first experiment. Resistivity values vary from about 3 $\Omega \cdot$ m in the underlying native soil to about 10^5 $\Omega \cdot$ m in parts of the upper pavement section. As expected, the overall pattern indicated drier conditions in the upper layers than in the subgrade soil.

The absolute images presented in Figure 7*a* are much better than those in Figure 4, and there is better correlation with the pavement structure. The plane images in Figure 7 are similar despite the different backfill materials (the 1–2 plane has existing material for backfill and the 3–4 plane has cement mortar backfill). The resistivity in the upper half of the AB is similar to that in the lower half of the ATPB. This pattern is repeated between the AB and the LTS as well as the LTS and native soil. The DGAC and ATPB layers show relatively high resistivity as expected. However, an unexpected low resistivity (that is, relatively wet condition) appears in the upper portion of the DGAC layer at the interface with the OGAC. The OGAC shows a surprisingly lower

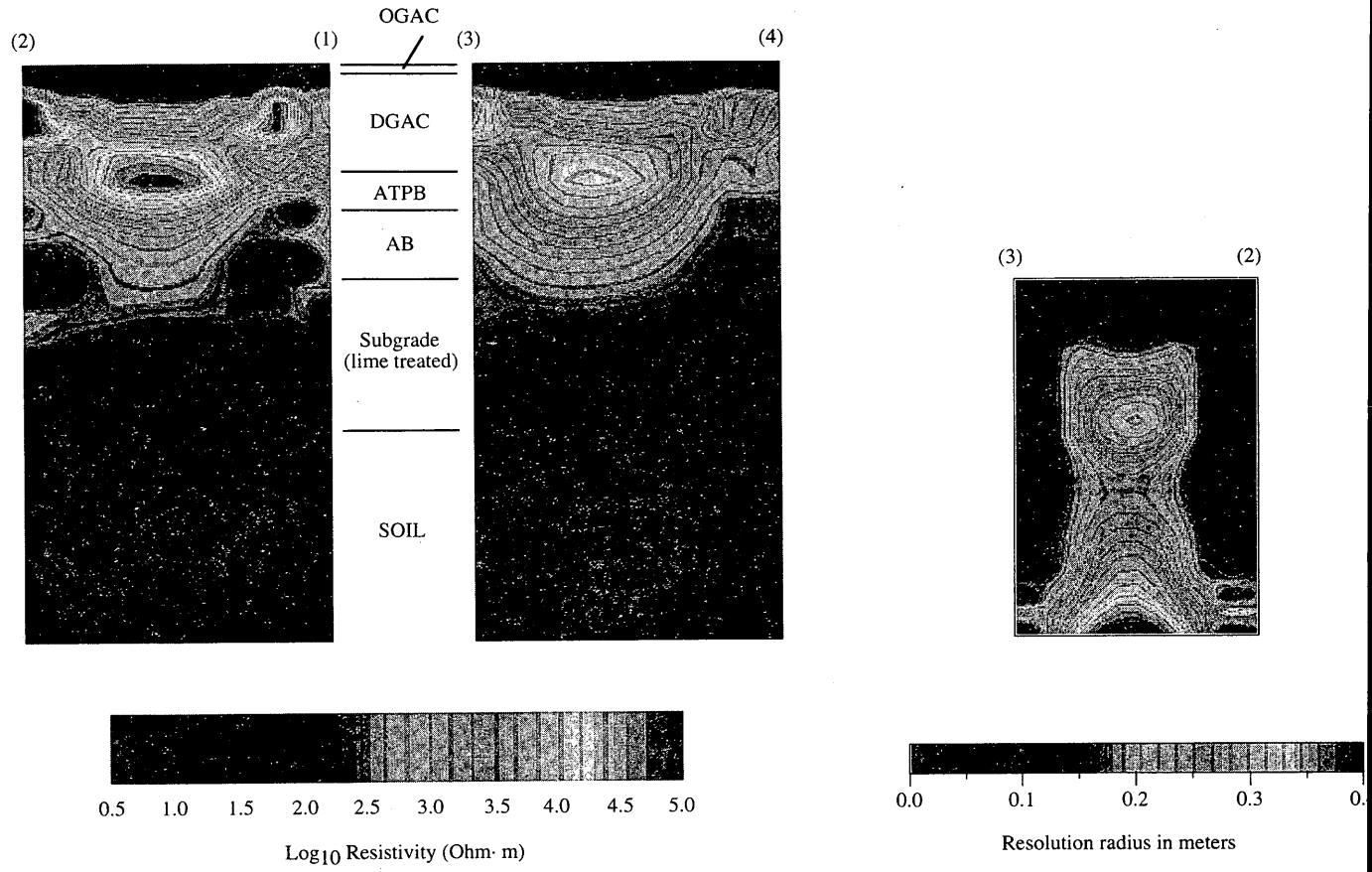

FIGURE 7 Plane images: (*left*), absolute ERT images of Planes 1–2 and 3–4; (*right*), resolution radius of Plane 3–2.

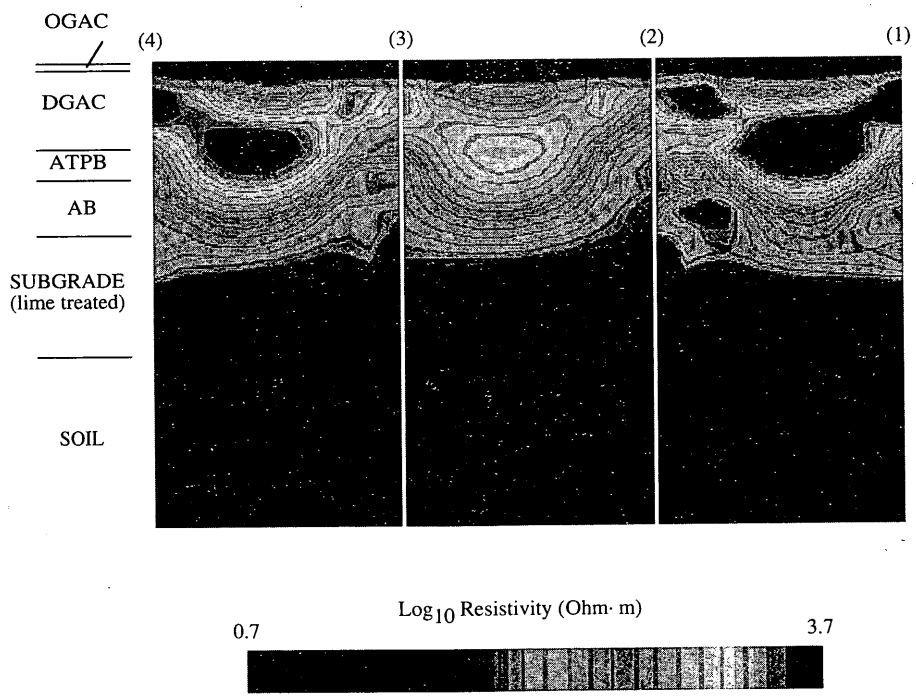

FIGURE 8 Baseline ERT images before water infiltration.

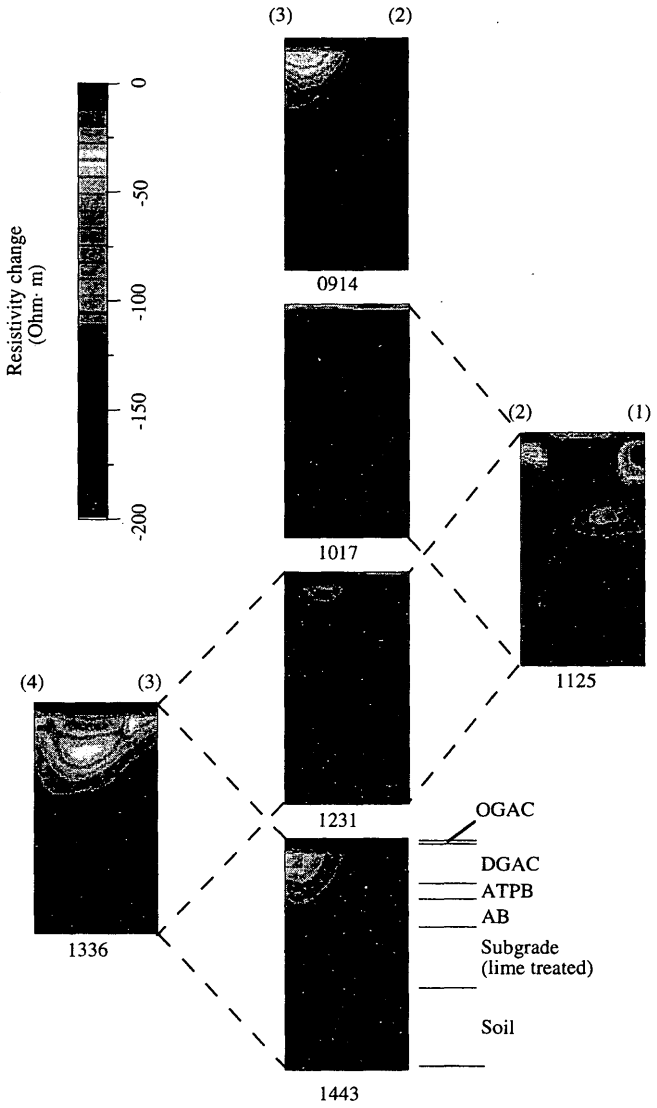

FIGURE 9 Comparison images during water infiltration.

resistivity than the DGAC despite sunny weather and a dry pavement surface that prevailed before and during data collection. One explanation for low resistivity at the DGAC/OGAC interface is vapor condensation. However, reasons for the low resistivity in the DGAC remain unknown until future research is done. The potential damages from high moisture content in these layers (e.g., asphalt stripping) justify further field study.

Figure 7*b* shows the resolution radius for the images in Figure 7*a*. The resolution radius can be thought of as a direct measure of the spatial resolution for the image: spatial resolution is better when the resolution radius is small and poorer when it is large. The resolution radius in this study varies from near zero to approximately 39.9 cm, whereas in Figure 4 it varies from about 10.2 to 50.8 cm. The resolution radius is better (smaller) near the electrodes and worse away from them because the pavement and soil materials are sampled more densely near the ERT arrays. In contrast to the first experiment, the improved resolution radius is largely a result of better-quality data and improved techniques.

Water Infiltration After obtaining good ERT images, an additional experiment was performed to measure horizontal and vertical water flow in the drained pavement section. The experiment was done in April 1993.

Before introducing water into the center hole (see Figure 6), ERT data were collected for baseline images. The baseline images of the 1–2, 2–3, and 3–4 planes, shown in Figure 8, match along their common edges and clearly show the expected resistivity structure (high resistivity in upper layers and low resistivity in the LTS and native soil). Like Figure 7*a*, the low resistivity is evident at the OGAC/DGAC interface.

The infiltration experiment was conducted during a period longer than 6.5 hr (from 8:40 a.m. to 3:00 p.m.) in which approximately 20.8 L of water was poured uniformly and slowly into the pavement through the center hole. Data were collected at several times during the infiltration period. The change in resistivity associated with moisture movement was imaged as a function of time. Four complete data sets were collected in the 2–3 plane (at 9:14 a.m. and 10:17 a.m. and 12:31 and 12:43 p.m.) because the researchers expected most of the water to drain through this plane. One data set was collected for the 3–4 plane at 1:36 p.m. and one for the 1–2 plane at 11:25 a.m. Because data collection required about 1 hr for each plane, the images represent time averages.

Water movement is inferred by contrasting the baseline data with those collected during water infiltration. Figure 9 shows a sequence of contrast images that show differences from the baseline conditions; that is, if there were no changes in resistivity because of water infiltration, the images would be a uniform single color. Progressive decreases in resistivity (i.e., increase in moisture) appear as progressively lighter as shown on the gray scale.

The sequence of images for the 2–3 plane shows decreased resistivity (interpreted as water flow) around the Borehole 3 at 9:14 a.m. At 10:17 a.m. this feature disappears, but ponding of water is evident across the section and in the LTS. By 12:31 p.m. this ponding disappears and there is more moisture movement around Borehole 3. Finally, at 2:43 p.m. there appears to be moisture movement around Borehole 3 much like that at 9:14 a.m. This sequence does not show a steady-state flow that is expected during slow constant infiltration.

The single image in the 3–4 plane at 1:36 p.m. shows moisture movement more evenly through the pavement section. This image matches well along the Borehole 3 edge with the 2–3 plane image at 2:43 p.m. The single image of the 1–2 plane at 11:25 a.m. shows moisture movement, although not as uniform, as the 3–4 plane at 1:36 p.m. The images in Figure 9 do not appear to show that infiltrated water drained preferentially to the shoulder through the 2–3 plane.

The sequence of images in this study shows that ERT can be used for further study related to drained pavement structures after improvement in some areas of ERT technology. For better understanding of the water flow in pavement system, it is recommended to improve ERT data collection system by decreasing the data collection time. In Experiment 2 the 1-hr data collection time is probably too long compared with the time scale of changes in the flow pattern in pavement structure. In addition, it would be valuable if data could be collected from multiple planes simultaneously and to provide better understanding of moisture movement in pavement system.

Finally, the following are concerns revealed during this study:

- There may be leaks or water movement between layers via boreholes,
- Image reconstruction introduces errors because it relies on two-dimensional analysis of three-dimensional water flow,
- Electrical properties (resistivity and change of resistivity) of pavement materials are not well known and correlation with moisture content is uncertain,
- Effects of water-soil-aggregate-asphalt binder interaction on water flow patterns are poorly understood, and
- All of the above are difficult to evaluate because of the long data acquisition time.

CONCLUSIONS AND RECOMMENDATIONS

ERT images showed moisture distribution and movement in pavement sections. These images correlate very well with known pavement structural sections where two different materials were used. Cold AC patching material was used successfully and is recommended as backfill in the ATPB and AC.

Further research to improve ERT technology will include laboratory testing of electrical properties of pavement materials, testing the water-soil-aggregate-asphalt binder interaction on water flow patterns, using reconstruction algorithms based on three-dimensional flow, and reducing data acquisition time.

Improved ERT technology will help pavement researchers and practitioners in many ways, such as visualizing moisture movement in pavement systems, understanding pumping mechanisms, determining traffic effects on water movement, and eventually designing pavement structures that are more resistant to water-induced damage.

ACKNOWLEDGMENT

Caltrans work was sponsored by FHWA, and LLNL work was performed under the auspices of the U.S. Department of Energy. The authors are grateful to John Carbino for fabricating the ERT probes and to Wayne Nakayama, John Morgan (District 4), and Kathy Coots (District 3) of Caltrans for their efforts in installing ERT probes.

REFERENCES

1. Daily, W. and E. Owen. Cross-Borehole Resistivity Tomography. *Geophysics*, Vol. 56, No. 8, Aug. 1991, pp. 1228–1235.
2. Daily, W., A. Ramirez, D. LaBrecque, and J. Nitao. Electrical Resistivity Tomography of Vadose Water Movement. *Water Resources Research*, Vol. 28, No. 5, May 1992, pp. 1429–1442.
3. Hohmann, G. W. Numerical Modeling for Electromagnetic Methods in Geophysics. In *Electromagnetic Methods in Applied Geophysics Theory*, Part 1, Vol. 3, (M.N. Nabighian, ed.), Society of Exploration Geophysicists, Tulsa, Okla., 1988, pp. 313–363.
4. Huebner, K. H. and E. A. Thorton. *The Finite Element Method for Engineers*. John Wiley and Sons, Inc., New York, 1982.
5. Wannamaker, P. E., J. A. Stodt, and L. Rijo. *PW2D Finite Element Program for Solution of Magnetotelluric Response of Two-Dimensional Earth Resistivity Structure*. Report ESL-158. University of Utah Research Institute, Salt Lake City, 1987.
6. LaBrecque, D. J. *Cross-borehole Resistivity Modeling and Model Fitting*. Ph.D. thesis, University of Utah, Salt Lake City, 1989.
7. Bard, Y. *Nonlinear Parameter Estimation*. Academic Press, San Diego, Calif. 1974, pp. 111–113.
8. Sasaki, Y. Model Studies of Resistivity Tomography Using Boreholes. Presented at the Society of Exploration Geophysicists International Symposium on Borehole Geophysics: Petroleum, Hydrogeology, Mining and Engineering Applications, Tucson, Ariz., Feb. 1990.
9. *Test Method 643*. Test Manual, Vol. 3. California Department of Transportation, Sacramento, 1978.

Publication of this paper sponsored by Committee on Pavement Monitoring, Evaluation, and Data Storage.